High pressure sensor based on fusion bonding

Birkelund, Karen; Sørensen, M; Chiriaev, S; Gravesen, P; Rasmussen, P. B.

Published in:
Semiconductor Wafer Bonding: Science, Technology, and Applications

Publication date:
2002

Document Version
Publisher's PDF, also known as Version of record

HIGH PRESSURE SENSOR BASED ON FUSION BONDING

K. Birkelund[1], M. Sørensen[2], S. Chiriaev[2], P. Gravesen[2], P.B.Rasmussen[2],
[1]Danfoss A/S, CAT, DTU, Bldg. 347, 2800 Lyngby, Denmark
[2]Danfoss A/S, 6400 Nordborg, Denmark
[1]e-mail: kb@cat.dtu.dk, http://www.danfoss.dk

ABSTRACT

In this paper we present a silicon based pressure sensor for high pressure applications. The sensor is based on fusion bonding and designed for a simple and a low-cost encapsulation scheme. The sensor can be designed for a maximum pressure in the range from 35 bar to 1500 bar and temperatures ranging from –40 °C to 120 °C and has a burst pressure exceeding 3000 bar. For proper performance of the sensor it is essential that the fusion bond interface is hermetic tight which will be one of the issues for discussion in this paper. Sensor design, fabrication and performance of the sensor will further be presented.

INTRODUCTION

Silicon pressure sensors are widely used in a large number of applications due to attractive performance characteristics such as sensitivity, long-term stability and last but not the least, cost effective manufacturing of pressure sensor dies.

It is, however, well known (1) that the encapsulation of conventional pressure sensor dies is delicate and expensive for many industrial and other demanding applications due to the inherent topology of conventional silicon chips. Stress de-coupling (2), media compatibility (3) and long term temperature stability are often issues, which must be dealt with either through unconventional chip-design or advanced packaging schemes.

By taking advantages of the nature of fusion bonding, we have realized a pressure sensor with an unconventional chip design, which deals with the above mentioned issues. The pressure sensor is shaped like a needle with the pressure sensitive region in one end, the contacts in the other end and interconnections along the needle. Figure 1 shows the concept of the sensor design and packaging scheme. The main advantages of this particular sensor design are that it offers a simple and compact packaging solution, which is an encapsulation unit sealed around the needle, separating the pressure sensitive region from the contact region. Because of the special needle shape the sensing region is stress decoupled from the package and it has good media compatibility. The pressure-exposed area is small, which implies that the pressure sensor has a high burst pressure.

The sensor is a piezo-resistive sensor made to operate in refrigeration- and fluid power systems with pressure range from 35 bar to 600 bar and temperatures raging from –40 °C to 120 °C. The pressure media are refrigerants and hydraulic oil which are light corrosive media concerning silicon.

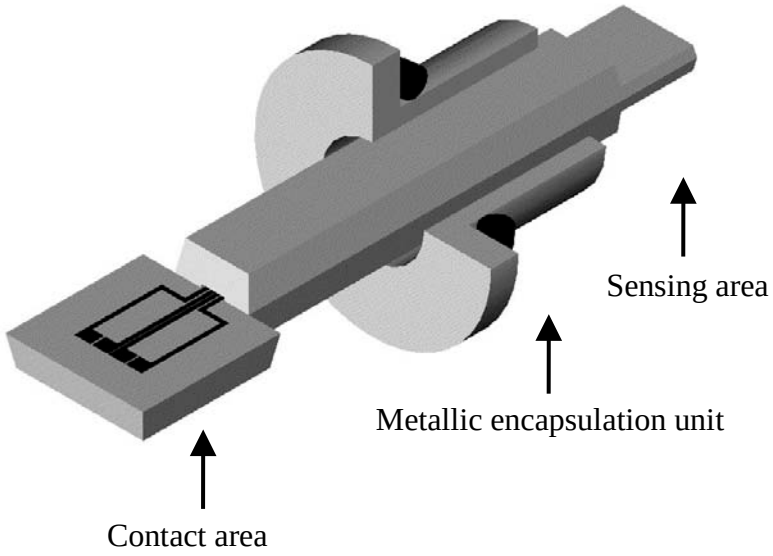

Figure 1. Illustration showing the concept of the pressure sensor design with (from left to right) bond-pad region, mounting region with a sealing encapsulation unit and the media exposed pressure sensing region. The contact pads and the piezo-resistors are connected by interconnections lying in the middle and along the needle.

DESIGN AND FABRICATION

The sensor can be realized either as an absolute sensor as described in ref. (4) or as a relative sensor where the pressure in the reference cavity is at atmospheric pressure. In this article we report on a relative sensor.

The realization of the sensor having this unconventional chip design has been made possible by the use of fusion bonding, where the electrical parts, such as piezo-resistors, contacts and interconnections, are di-electrical isolated, buried in silicon oxide and sandwiched between to silicon wafers. The needle shape is thereafter etched in an an-isotropic etch and an optional protective coating can be deposited on wafer scale to protect the needle against corrosive media.

The electrical part is realized in a top silicon layer of an SOI-wafer. The SOI-wafer is 350 μm thick with a 200 nm thick buried SiO_2 layer and a 1 um thick top silicon layer. First the electrical part are defined by a local oxidation process, where the silicon between piezo-resistors, interconnections and contacts are consumed during a oxidation process using silicon nitride as a masking material. Then the nitride is removed and an oxide etch ensure that the height of the oxide is lower than the overall level of the wafer surface. A final thermal oxidation process seals the electrical parts in oxide. The areas between the electrical parts then appear as 2000 Å deep recesses all in oxide. In order to achieve the required conductivity of the piezo-resistors, interconnections and contact pads a Boron implantation is made. The implantation dose for the piezo-resistors is $5 \cdot 10^{14} cm^{-2}$. To achieve a low resistance of the interconnections and contact pads these are given a

Boron dose of $1.5 \cdot 10^{16}$ cm^{-2}, while the piezo-resistors are protected with a 700 nm thick aluminum mask. The piezo-resistors are placed in a Wheatstone bridge configuration and will be situated on the backside of the pressure sensitive membrane. The bridge is connected to the contact pads by the feed-through interconnections. The electrical part is illustrated on Figure 2.

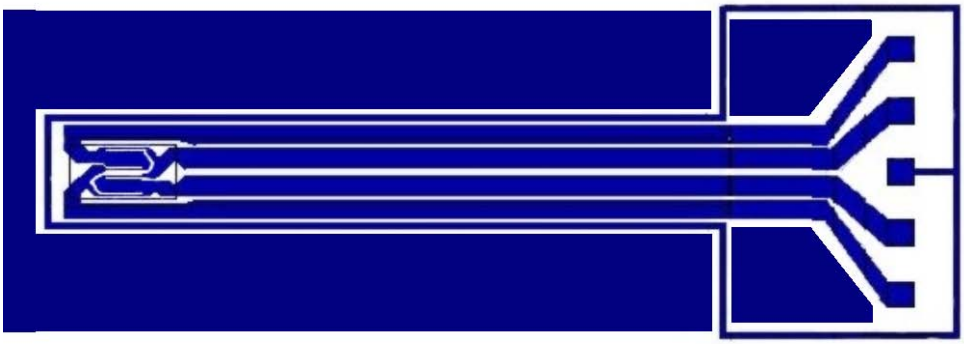

Figure 2. Piezo-resistors (left) in a Wheatstone bridge configuration are connected to the contact pads (right) by the feed-through interconnections (middle). The white areas indicate the local oxidized areas and appear as 2000 Å deep recesses.

On an other wafer, which is a standard double polished (100) wafer, 2.5 μm deep recesses are etched in a KOH etch. Two recesses are made for each sensor element. One recess will define the membrane area and form a reference pressure cavity, and the second recess will form a sealed cavity for protection of the contact pads during subsequent etching and coating processes on the fusion bonded wafer stack.

FUSION BONDING

In order to fusion bond the two processed wafers two criteria have to be fulfilled. First, the bow of the wafer should be minimized. Processed wafers often experience a built in stress due to unbalanced or structured thin film layers giving rise to a considerably bow of the wafers. If the bow is sufficiently large the forces acting on the wafer are larger and opposite directed than the bonding forces responsible for the spontaneous pre-bond and the wafers tend to de-bond. Based on experience the bow of the wafers should be less than 5 μm, in order to obtain a sufficiently good pre-bond. The SOI-wafers have an initial bow of about 25 μm due to a compressive stress of the buried oxide in the SOI-wafers. During the wafer processing, with different layers of oxide, silicon nitride, boron implantation and various high temperature treatments, the stress of the wafer change significantly. To achieve a final minimal bow of the wafers the thickness of an oxide layer on the backside of the wafers are adjusted as the last process step prior to the bonding process.

Secondly, the surfaces to bond should be smooth and clean since one single particle on the bonding surface may deteriorate yield significantly. Therefore the wafers are cleaned thoroughly prior to bonding by using a modified IMEC clean [5]. First, the wafers are soaked for 5 min in a 80 °C H_2O_2:H_2SO_4 solution, then for 100 s in a solution of DI water, hydrofluoric acid and isopropyl alcohol, and finally for 20 min in H_2O_2:H_2SO_4 at

80 °C. Each treatment is followed by a 5 min rinse in DI-water and finally they are dried in a spin dryer.

The two wafers are aligned and pre-bonded in an Electron Vision aligner. Inspection in an infrared camera reveals whether the wafers are properly bonded or not. Wafers with large voids can then be separated, cleaned and bonded again. Wafers, which are properly bonded, are given a high temperature treatment of 4 hours at 1000 °C in a wet oxidation process in order to strengthen the bond and to grow an oxide used as a masking material in a later etch process. Pull tests have shown bond strength of about 25 MPa with a standard deviation of 9 MPa.

KOH-ETCHING

After fusion bonding the needle sensor is released by KOH-etching. At the same time the membrane is defined. The complete outer structure of the needle is defined using a two step mask-less etch in KOH as described elsewhere (6). During the etching process the membrane is protected by a 1 μm thick oxide layer and the rests of the sensor is protected by a 100 nm thick Si_3N_4 layer. The wafer is etched in KOH to a depth corresponding to the desired membrane thickness. Subsequently the oxide on the membrane is stripped followed by another KOH etch etching all the way through the wafers to release the sensors. The two etching times depend on the desired membrane thickness.

This etching scheme takes advantage of the fact that, when the <100> direction is etched an-isotropic in KOH after a masked etch, the intersections between the {100} planes and the {111} planes are cut by the {311} planes. The {311} planes etch about 1.8 times faster than the {100} planes in a 28 wt% KOH (6). The above outlined etching scheme results in a cross section of the membrane, as shown in figure 3. Different versions of the sensor can be designed for a maximum pressure ranging from 35 bar to 1500 bar by varying the membrane thickness from 50 μm to 300 μm respectively.

In order to protect the contact pads during the processing and still be able to get access to the contacts after the last processing step a protecting membrane is made. The protecting membrane is made during the KOH etch, where the etching is stopped on a 5 μm thick boron etch stop layer in the cavity covering the contact pads, as shown in figure 3a. The membrane is sufficiently rigid to sustain the processing and it is easily removed mechanically when access to the contact pads is required. After removing the protecting membrane, aluminum is evaporated onto the contacts through an external shadow mask. In order to achieve good contacts the wafer is annealed for 30 min at 400 °C. The sensors are then ready for dicing, packaging, interconnection and calibration.

A completed sensor is shown in figure 4. The needle is 5 mm long, 1 mm wide and 700 μm thick. The membrane is 400 μm by 800 μm and the electrical contact area is 2 mm by 2.5 mm.

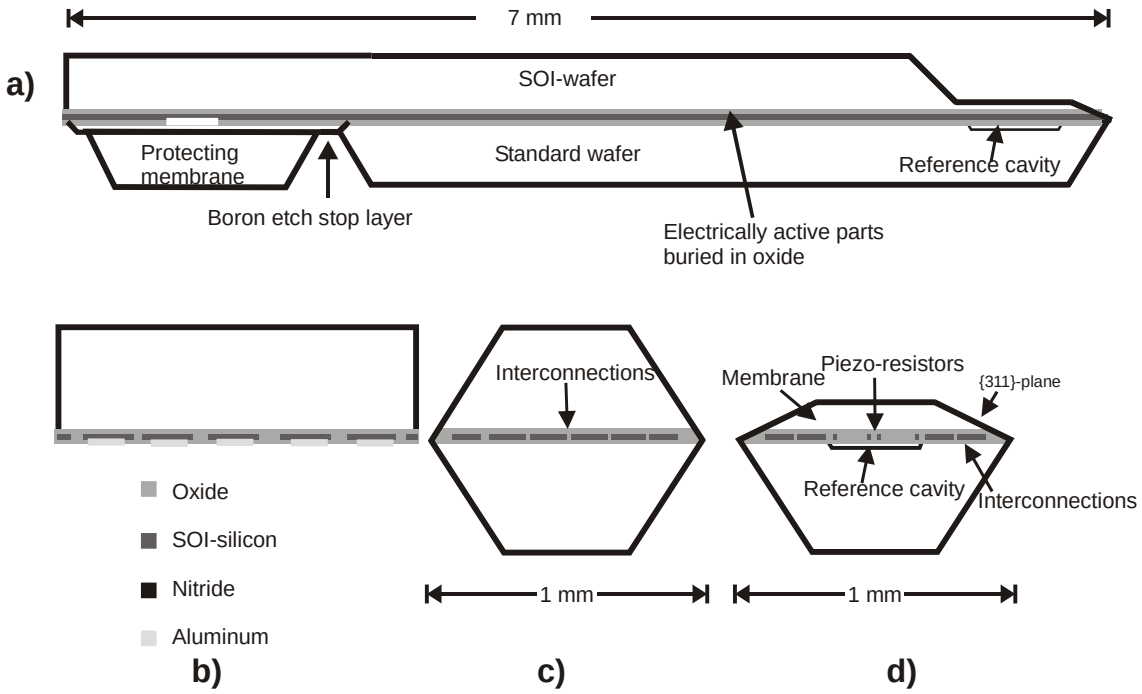

Figure 3. a) Cross sectional drawing of the sensor along the needle. The protecting membrane protects the contact pads during processing and is removed prior to metallisation of the contacts. b) Cross sectional drawing of the contact area after removal of protecting membrane and evaporation of aluminum. c) Cross sectional drawing of the needle with the interconnections covered with oxide. d) Cross sectional drawing of the membrane area showing how the membrane will look like after the two etching steps in KOH. The piezo-resistors and interconnections are covered with oxide.

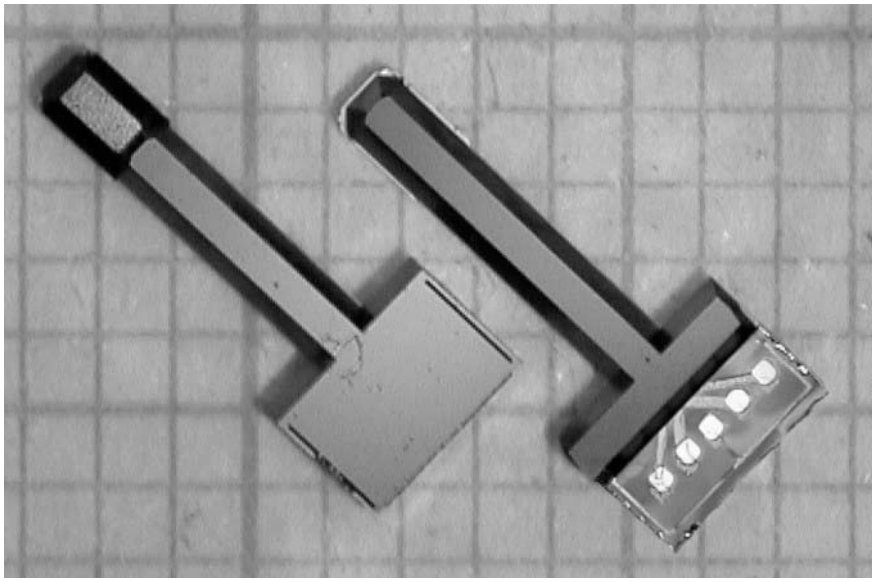

Figure 4. Photos of the pressure sensor on a piece of millimeter paper. Left: Shows the membrane side of the sensor with the membrane area at the upper end of the needle. Right: Shows the contact side of the sensor with the bond pads. The total chip size is only10 mm^2.

PERFORMANCE

Sensors with 50 µm thick membranes have been tested under pressure ranging from 0 bar to 30 bar at five different temperatures. The graph in figure 5 shows the output of four sensors as a function of pressure at 25 °C. Within this pressure range and at an excitation voltage of 5V the sensors exhibit a linear output with a typical sensitivity of about 0.9mV/V/bar. Offsets are typically in the range –21mV to 37 mV. The output voltage, V_{out}, can to first order be described by following expression:

$$V_{out} = V_{in}\left[Offset + TCO \cdot (\Delta T) + G(T)\varepsilon_{span} \frac{P - P_0}{P_f} \right] \qquad [1]$$

where V_{in} is the excitation voltage, TCO is the temperature coefficient of the offset, ΔT is the temperature difference, ε_{span} is the average strain at full span pressure, P is the applied pressure, P_0 is the pressure in the reference cavity and P_f is the full span pressure. $G(T)$ is the gauge factor and given by:

$$G(T) = G(T_0)\left(1 + TCG \cdot (\Delta T) + TCG_{nl} \cdot (\Delta T)^2\right) \qquad [2]$$

Here TCG and TCG_{nl} are the temperature coefficient of G and the non-linearity of TCG respectively.

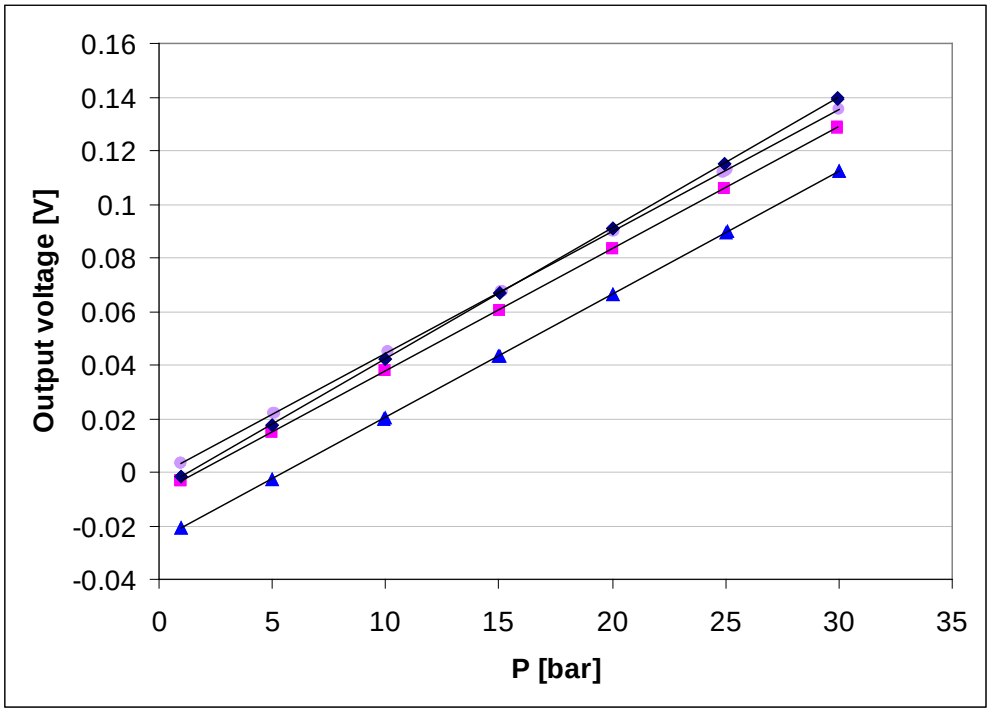

Figure 5. Output voltage plotted with applied pressure for four 30 bar sensors at 25 °C and at 5V excitation voltage. A trend line is drawn for each sensor.

In order to extract the coefficient in equation [1] the data is normalized to the excitation voltage and it is assumed that the pressure in the reference cavity is constant within the short time it takes to carry out the measurement. By fitting the measured data to equation [1] by least square fitting the coefficients in equation [1] are extracted. Typical values of the coefficients are listed in table 1. In general the sensors behave as expected.

Table 1. The coefficients estimated for four different 30 bar sensors.

Offset	$-1.78\cdot10^{-3}$	$-3.20\cdot10^{-4}$	$-4.14\cdot10^{-3}$	$6.06\cdot10^{-4}$
TCO (1/°C)	$-1.00\cdot10^{-5}$	$-9.82\cdot10^{-6}$	$-6.58\cdot10^{-6}$	$-1.48\cdot10^{-5}$
$G\varepsilon_{span}$	$2.72\cdot10^{-2}$	$2.85\cdot10^{-2}$	$2.66\cdot10^{-2}$	$2.64\cdot10^{-2}$
TCG (1/°C)	$-2.67\cdot10^{-3}$	$-2.78\cdot10^{-3}$	$-2.68\cdot10^{-3}$	$-2.73\cdot10^{-3}$
TCG_{nl} (1/°C^2)	$7.76\cdot10^{-6}$	$8.26\cdot10^{-6}$	$6.61\cdot10^{-6}$	$7.42\cdot10^{-6}$

LEAK TEST

However, it is essential that the fusion bond is sufficiently tight for the sensor to perform for at least 10 years. The maximum acceptable change in reference pressure is 0.1% of the full scale pressure per year. This means leakage from the ambience into the reference cavity may not exceed 10^{-16} Pa·m^3/s (10^{-15} mbar·L/s) for our 30 bar sensors, with a reference cavity volume of only 800 pL. The specific leak rate, Q_{leak} is given by:

$$Q_{leak} = \frac{\mathrm{d}P_0}{\mathrm{d}t} \cdot V_{cavity} \qquad [3]$$

where P_0 is the reference pressure inside the cavity and V_{cavity} is the volume of the pressure reference cavity. We assume that the $\mathrm{d}P_0/\mathrm{d}t$ is constant, i.e. that the leakage is so small that the reference pressure does not change significant. The time constant τ for the pressure increase in the cavity is given by:

$$\tau = \frac{P_f V_{cavity}}{Q_{leak}} \qquad [4]$$

where P_f is the full span pressure. For a 30 bar sensor with a leak rate smaller than 10^{-16} Pa·m^3/s this corresponds to a characteristic time of more than 1000 years.

In order to measure leak rates the following experiment was carried out. Four 30 bar sensors were exposed to 30 bar for a period. The leak tests have been carried out with three different gasses. First the sensors were exposed to air for a week, then with helium for 24 hours and finally the sensors were exposed to argon for a week. During the test

period the ambient temperature and the applied pressure were controlled in an open loop and monitored together with the output voltage of the sensors every 15 minute. The output voltages were normalized to T_0 = 23 °C and P = 30 bar. On the graph in figure 6 the output voltage, the compensated output voltage and the pressure is plotted with time during the leak test with ambient air.

Using the former extracted coefficients listed in table 1 the relation between change in output voltage and change in the reference cavity with time at constant temperature and constant ambient pressure is then given by:

$$\frac{\mathrm{d}V_{out}}{\mathrm{d}t} = -\frac{G\varepsilon_{span}}{P_f} \cdot \frac{\mathrm{d}P_0}{\mathrm{d}t} \qquad [5]$$

From the compensated measured data from the leak experiment it is now easy to determine $\mathrm{d}P_0/\mathrm{d}t$ from equation [5], and thereby the leak rate using equation [3].

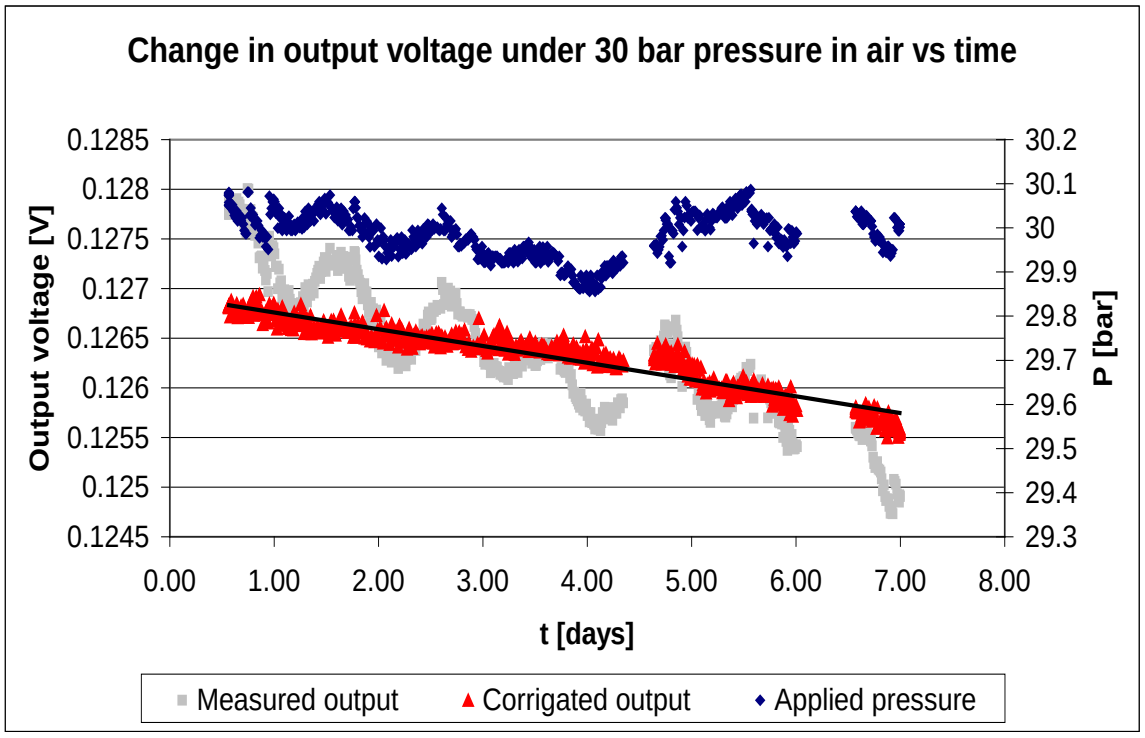

Figure 6. The measured output voltage, the compensated output voltage with trend line and applied pressure plotted with time.

The estimated leak rates are listed in table 2. The experiment with helium was stopped after 24 hours because of the considerably large leak rate. Still seven days after the leak test with helium the pressure inside the cavity was still about 3 bar, falling about 0.5 bar per day. Even when the sensors were exposed to argon at 30 bar pressure, the total pressure inside the cavity was decreasing, i.e. more helium was diffusing out than argon was entered in the cavity. This indicates that the flow depends on the partial pressure of the

gasses and not the total pressure. For that reason the leak test with argon was carried out with four new sensors.

Table 2: Typical leak rates from the ambience into the pressure reference cavity for three different gasses.

Gas	Leak rate ($Pa \cdot m^3/s$)				Average
Ambient air	$3.4 \cdot 10^{-14}$	$3.6 \cdot 10^{-14}$	$4.7 \cdot 10^{-14}$	$3.7 \cdot 10^{-14}$	$3.9 \cdot 10^{-14}$
Helium	$3.5 \cdot 10^{-12}$	$5.4 \cdot 10^{-12}$	$1.3 \cdot 10^{-11}$	$6.1 \cdot 10^{-12}$	$7.0 \cdot 10^{-12}$
Argon	$2.1 \cdot 10^{-14}$	$2.4 \cdot 10^{-14}$	$4.8 \cdot 10^{-14}$	$1.7 \cdot 10^{-14}$	$2.8 \cdot 10^{-14}$

The leak test with air shows, that the four sensors have a specific leak rate between $3.3 \cdot 10^{-14}$ $Pa \cdot m^3/s$ and $4.7 \cdot 10^{-14}$ $Pa \cdot m^3/s$. This corresponds to a change in reference pressure of 46%-63% of full scale per year and a time constant of 1.6 – 2.2 years. When air was changed with helium the four sensors had a specific leak rate between $3.5 \cdot 10^{-12}$ $Pa \cdot m^3/s$ and $1.3 \cdot 10^{-11}$ $Pa \cdot m^3/s$ - the leak rates increase by between 103 times and 276 times. The leak rates in ambient air and argon are in the same order of magnitude.

If we assume that the leak into the cavity simply comes from diffusion through the silicon membrane then we are able to calculate the time constant as:

$$\tau = \frac{V_{cavity} \cdot t}{K_{\mathrm{He}} \cdot A} \qquad [6]$$

where t indicates how thick the membrane is, K_{He} is the permeability and A is the area of the membrane. Based on high temperature diffusion constant, we made a rough estimate of helium permeation at room temperature. With an estimate for K_{He} between 10^{-19} m^2/year and 10^{-23} m^2/year (7), and with a sensor geometry of V_{cavity} = 800 pL, d = 50 µm and A = 400 µm · 800 µm we get τ between $1.3 \cdot 10^9$ years and $1.3 \cdot 10^{13}$ years. It is obvious that the leakage we observe cannot be diffusion through the silicon membrane.

DISCUSSION

The observed leaks can be caused by one of three types of transport mechanisms of small leaks. The tree models are illustrated in table 3 below.

Table 3: Possible transport mechanisms of small gas leaks extracted from (10) and (11).

Transport mechanisms of small leaks			
Type of flow or transport	Pressure scaling factor	Gas dependent scaling factor	Geometrical scaling factor
Laminar flow (collective flow with parabolic velocity profile) 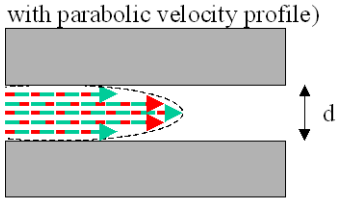	$\frac{(P_{high}^{\ 2} - P_{low}^{\ 2})}{2}$ (Total pressure)	$\frac{1}{\eta(\sigma, m, T)}$ (Viscosity)	$\frac{\pi}{128}\frac{d^4}{L}$ (L>>d)
Molecular flow (Random walk with few intermolecular collisions) 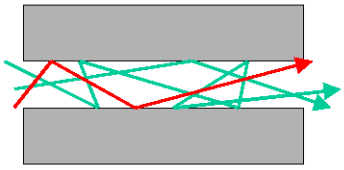	$\frac{P_{high} - P_{low}}{2}$ (Partial pressure)	$\bar{v}(m,T)$ (Mean velocity)	$\frac{\pi}{12}\frac{d^3}{L}$ (L>>d)
Permeation through the bonding oxide layers and their interface 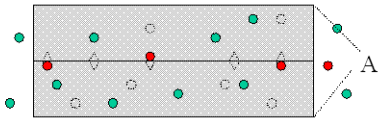	$P_{high} - P_{low}$ (Partial pressure)	$K_{gas}(T)$ (Permeability)	$\frac{\pi}{4}\frac{d^2}{L} = \frac{A}{L}$

We have already concluded that the flow depends on the partial pressure and not on the total pressure. This fact excludes laminar flow.

Let us assume that we have a molecular flow. In that case we would expect $Q_{He} \approx 3Q_{Ar}$ in the leak channel(s), because the mean velocity of helium molecules are about three times bigger than the mean velocity of argon. From our experiments we see that $Q_{He} \approx 250 \cdot Q_{Ar}$, which indicates that the most of the Helium leak is caused by permeation. Back calculation of leaks and relevant dimensions result in the following (table 4):

Table 4: Back calculation of leaks and equivalent "channel" dimensions under the assumption of molecular flow of Argon in one dominating or 1000 parallel "channels"

Leak component	Value in	Diameter of one dominating channel	Diameter of 1000 parallel channel
Argon leak (molecular)	$2{,}8 \cdot 10^{-14}$ Pa·m³/s	75 Å	7,5 Å
Helium leak (molecular)	$8{,}4 \cdot 10^{-14}$ Pa·m³/s	75 Å	7,5 Å
Helium leak (Permeation)	$6{,}9 \cdot 10^{-12}$ Pa·m³/s	-	

Now, even if the back calculated dimensions shown in table 4 are theoretically possible, we will reject the hypotheses of molecular flow on the basis of the extreme small dimensions, which are of same order of magnitude as molecular binding length.

Hence, we conclude that the leak is caused by permeation through the bulk of the bonding oxide layers or through defects of their interface. If the leak is caused by the permeation through the bulk, Q_{He} is given by:

$$Q_{He} = (P_{high} - P_{low}) \cdot \frac{A}{L} \cdot K_{He} \qquad [7]$$

The permeability of fused silica to helium is $7.5 \cdot 10^{-13}$ m^2/s (8). For the given geometry of the sensor (L=150 μm, A=1.1 μm· 5000 μm) and at a pressure difference of 29 bar, it gives $Q_{He} = 8 \cdot 10^{-11}$ $Pa \cdot m^3/s$. We detected a leak rate of about $7 \cdot 10^{-12}$ $Pa \cdot m^3/s$, that is11 times smaller than the expected leak rate through fused silica. The bonding layers in the sensor presented here consist of thermally grown SiO_2. It is therefore reasonable to assume that the permeability of helium through the thermally grown SiO_2 is less than through fused silica at room temperature, due to a higher stress in thermally grown SiO_2.

On the other hand, in the case where the sensors were exposed to argon, we detected a 250 times lower leak rate compared to that for helium. It is known however, that the diffusion of helium in fused silica at room temperature is at least 10^{10}times bigger than the diffusion of argon (9). This indicates that the detected leak rate of argon may be caused only by permeation through interface defects. In the case of He, the leak may occur through both the bulk of the bonding oxide layers and their interfaces.

CONCLUSION

We have designed and fabricated a high-pressure silicon sensor based on fusion bonding with lateral feed-through and a simple packaging. The sensor is a relative pressure sensor with piezo-resistive read out designed for refrigeration- and fluid power systems. The needle shape of the sensor has several advantages. It allows a compact and cheap packaging solution, it gives the sensor a high burst pressure of about 3000 bar, and it facilitates a favorable de-coupling of the sensor membrane from packaging stress. The sensor can easily be realized to operate at a pressure up to 600 bar by varying the membrane thickness and may be realized for even higher pressures with minor changes in geometry. The overall performance of the sensors was found close that expected. An essential issue for proper performance is that the fusion bond is hermetic to a leak level of 10^{-16} $Pa \cdot m^3/s$. Leak tests reveal that this is not the case and that leaks are caused by permeation through the bonding structure. Penetration through both the interface defects as well as through the bulk of thermal SiO_2 may provide the measured leak rates in the case of He. In the case, of air and argon permeation through the interface defects seems to be the dominant leak mechanism.

In order to make a sensor that will meet the leak requirement several attempts could be made. First of all, efforts should be made to optimize the fusion bonding process in order to minimize the permeation of molecules through the interface defects. The sensor can never be made as an absolute sensor hermetic tight to helium, due to the very high permeability of helium through SiO_2. Secondly, the sensors can be made less sensitive to leaks by increasing the volume of the reference cavity. By increasing the depth of the cavity to 25 μm the maximum acceptable leak can be increased by a factor of 10.

ACKNOWLEDGMENTS

The work has been done whit-in SESIBon (Sensor Encapsulation by Silicon Bonding) and partly founded by the European Competitive and Sustainable Growth Programme (Contract number: G1RD-CT99-0002). It has further been part of the SUM project (No. 1999-603/40001-13) financially supported by the Danish Agency for Trade and Industry Finally we would like to thank Ole Hansen at Mikroelektronik Centret, Technical University of Denmark and Jørgen Trelle Petersen at Danfoss A/S, Denmark for fruitful and interesting discussions.

REFERENCES

1. R. de Reus, C. Christensen, S. Weichel, S. Bouwstra, J. Janting, G. Friis Eriksen, K. Dyrbye, T. Romedahl Brown, J.P. Krog, O. Søndergård Jensen, P. Gravesen, *Microelectronics Reliability*, **38**, 1251-1260, (1998).

2. V.L.Spiering, S. Bouwstra, R.M.E.J Spiering, *Sensors and Actuators A*, **39,** 149-156 (1993).

3. G.F.Eriksen, *Proc. Of The 10th International Conference on Solid-State Sensors and Actuators (Transducers '99), Sendai, Japan, June7-10, 366-369, (1999).*

4. K.Birkelund, P. Gravesen, S. Shiryaev, P. Brandt Rasmussen, M. Dall Rasmussen, Sensors and Actuators A**, 92/1-3**, 16-22, (2001).

5. M.Meuris, P.W. Mertens, A. Opdebeeck, H.F. Schmidt, M. Depas, G. Vereecke, M.M Heyns, A. Philipossian, *Solid State Technology*, 109-113, July (1995).

6. X. Li, M. Bao, S. Shen, Sensors and Actuators A**, 57**, 47-52, (1996).

7. A.S. Grove, *Physics and technology of semiconductor devices*, p.40, fig. 3.4, John Wiley & Sons, New York (1967).

8. *Introduction to Helium Mass Spectrometer Leak Detection*, p. 49, Varian, Palo Alto, (1980).

9. M.R.Carroll and E.M. Stolper, *Geochim. Cosmochim. Acta*, **55**, 217, (1991).

10. S. Dushman and J.M. Lafferty J.M., S*cientific Foundation of Vacuum Technique*, Second edition, New York: John Wiley Sons, (1962).

11. W.F. Hughes and J.A. Brighton, *Fluid Dynamics*, New York: Schaum Publ. (1967).